

## Geochemistry of Economic Heavy Minerals from Rosetta Black Sand of Egypt

A.A. El-Kammar, A.A. Ragab\*, and M.I. Moustafa,\*

Geology Department, Faculty of Sciences, Cairo University, Giza, Egypt

\* Nuclear Materials Authority, P.O. Box 530 Maadi, Cairo, Egypt

Received: 28/ 03/2010

Accepted: 26/ 06/2010

*Abstract.* The potential heavy minerals content of the black-sand resources in Rosetta is investigated using optical microscopy, X-ray diffraction, scanning electron microscope, electron-microprobe analysis and inductively coupled plasma-mass spectrometry. The separation of individual minerals was done by wet-gravity and applying magnetic and electric approaches. The composition and morphology of the studied heavy minerals such as zircon, monazite, garnet, magnetite, ilmenite and rutile are compared with their equivalents in the Nile sources to elucidate their fate during the long transportation. Shukri's samples of the Nile sediments that were collected and studied during the mid-twentieth Century are adopted for this comparison. Generally, mineral grains turn to be polished and free of contamination upon long transportation while others are entirely lost before reaching the influx. Even the ultrastable minerals such as zircon and monazite experienced some changes in their chemical composition during transportation. The REE geochemistry suggests that the coarse grained zircon was possibly derived from highly fractionated and altered pegmatitic rocks of White Nile proximity while the fine grained variety was derived from the Ethiopian hinterlands. Two monazite varieties are distinguished, namely; Ce-monazite and Th-monazite, however, the extreme Eu deficiency ( $\Delta\text{Eu} = <0.1$ ) is used to assign derivation from highly fractionated felsic sources. Garnet belongs essentially to almandine variety is derived from metamorphic rocks such as the prevailing two-mica schist of White Nile provenance. The opaque minerals; magnetite, ilmenite and rutile have nearly flat chondrite-normalized REE patterns but with slight enrichment in LREE. These minerals are good indicators of the volcanic source of the Ethiopian plateau. Few gold grains have been detected in the high grade cassiterite concentrate with average concentration of 7780 ppb Au. The

radioactivity in the studied black sands is essentially attributed to both uranium and thorium series mostly related to monazite, zircon, garnet and ilmenite.

## Introduction

Black sand is a heavy, glossy, partly magnetic mixture of usually fine sand, found as part of a placer deposit. The mechanical concentration of resistant heavy minerals takes place in the beach environment, mostly under high energy conditions and their petrological composition is mostly controlled by the original source rocks (Basu and Molinaroli, 1989). The River Nile and its tributaries drain minerals of different sources along its course from the central and eastern parts of Africa in the south to the Mediterranean Sea in the north. The Nile sediments are derived mainly from three main basins, namely; White Nile, the Blue Nile-Atbara and north of Atbara basins. The trace elements content of the heavy minerals fraction of the Nile sediments reflect the nature of its mineral composition and their source rocks (El-Kammar, *et al.*, 1992).

The provenances of the Blue Nile and Atbara Rivers, in their upper courses, are mildly alkaline to tholeiitic basalts and rhyolitic ignimbrites (Wolfenden, *et al.*, 2005). According to Garzanti, *et al.*, (2006) the Blue Nile levee deposits consist mainly of mafic volcanic grains with subordinate quartz, plagioclase, K-feldspar and biotite. The heavy minerals portion is dominated by augite, with minor opaques, hornblende and epidote. Atbara levee deposits are dominated by volcanic detritus. The prevalence of clinopyroxene and olivine suggests greater contributions from volcanic rocks, including olivine-rich basalts (Pik, *et al.*, 1998). Bar deposits also mainly consist of basaltic fragments besides augite, plagioclase and quartz grains.

According to Garzanti, *et al.*, (2006), the heavy minerals of Gash sands include epidote, amphiboles and augite. The Gash levee shows a small concentration (0.1%) of transparent heavy minerals including monazite. In contrast, the White Nile drains amphibolite associated mainly with quartz, and the heavy minerals; zircon, rutile, garnet, kyanite, staurolite and titanite. The levee and bar deposits of the two main White Nile branches in southern most Sudan (Baro-Sobat and Bahr El-Zeraf) contain only 0.1% of transparent heavy minerals including monazite. In their middle course, the Blue and White Rivers gorges cut

across the underlying pre-rift sedimentary succession (Mesozoic limestone, sandstone and local Permian tillite) and then across the Pan-African basement units, which are more widely exposed and display increasing metamorphic grade towards the southwest (Tadesse, *et al.*, 2003).

The Egyptian black sand comprises huge reserves of economic metals-rich heavy minerals that include ilmenite, magnetite, garnet, zircon, rutile and monazite. These deposits occur as beach sediments and coastal sand dunes (Fig. 1). Several mineralogical and radiometric investigations have been carried out on these sands including; El Shazly, (1965); El Shazly, *et al.*, (1981); Anwar and Bousiely, (1970); and Dabbour, (1997).

This paper summarizes important original data of electron microprobe analysis (EMPA), scanning electron microscope (SEM) and inductively coupled plasma–mass spectrometry (ICP-MS) on some heavy minerals separated from the black sands occurring in Rosetta prospect as well as source areas. The objective of this study is to improve the available data base on the composition, use, origin and provenance of these potential minerals.

### Geographical Features

Black sand deposits occur along the Egyptian northern Mediterranean coast from Rosetta to Rafah (Fig. 1). The concentration of the heavy minerals comprising these deposits varies from place to place. The greatest concentrations are located close to the outlets of the River Nile.

The beach area of Rosetta contains most of the economic heavy minerals reserves of black sand in Egypt owing to their great extension and high grade (Dabbour, 1995). The beach sand placer deposits of Rosetta area either in its western or eastern sides are almost flat with alternate dark and light colored bands. These sands contain about 3% of some important economic minerals, namely; magnetite, ilmenite, zircon, rutile and monazite.

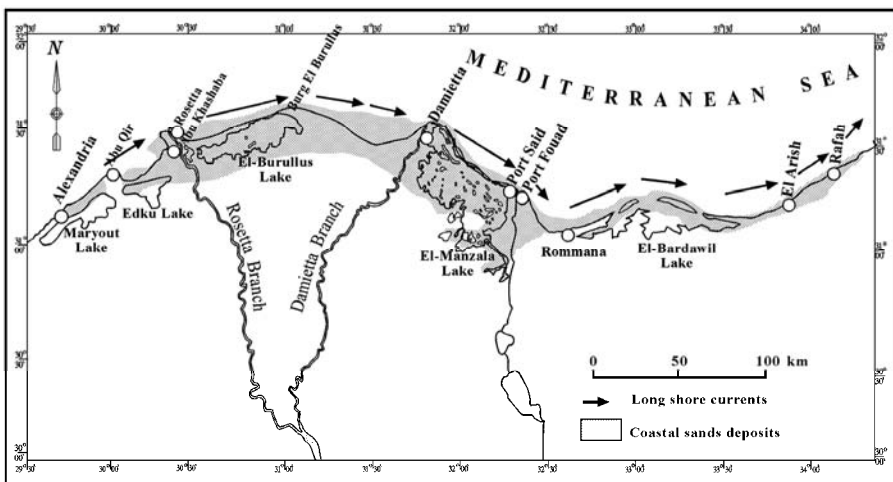


**Fig. 1. Location map.**

The most important surficial feature of the black sands of Rosetta is the presence of the naturally formed concentrated lenses, which can be exploited for their content of zircon and rutile. Several studies were carried out on these parts of the beach. The prominent studies include El Hadry (1988 and 1998) and Moustafa, (1995).

### **Sampling, Separation and Analytical Methods**

This study focuses on some economic heavy minerals, namely; zircon, monazite, garnet, magnetite, ilmenite, rutile, cassiterite and gold. Seven samples representing the study area (about 2km<sup>2</sup>) were collected from the highly concentrated black sand on a grid pattern of 200m - 100m and the drilling to 5 meters depth. In the present study, collaborative techniques have been employed for concentration and separation of the economic heavy minerals.

The separation was done by the Wilfley shaking tables for wet-gravity concentration. The Carpco high-tension roll-type electrostatic separator-model HP-167 and model Hp-114 was used for high tension electrostatic separation and the Carpco magnetic separator, model-MLH (13) 111-5 for magnetic separation. High-purity concentrate of individual economic minerals are obtained by using wet-gravity concentration, high-tension electrostatic separation and both low and high intensity

magnetic separation at the optimum adjustments of operating conditions. Details on the separation process are given by Moustafa, (1995). The significant difference in specific gravities between gangue minerals such as quartz (2.65) and green silicate minerals (3.5, in average) and the economic minerals such as monazite (5.2), ilmenite (4.7), zircon (4.6), rutile (4.2), garnet (4.0) and magnetite (4.9) has been utilized. The difference in the magnetic susceptibilities between economic minerals has also been utilized.

The bulk of the economic minerals concentrate is separated into two major fractions, namely; magnetic and non-magnetic. Each of these two major fractions has been further classified according to their electrical conductivity. The conductor rutile is separated from the non-conductor zircon and the conductor ilmenite is separated from the non-conductor garnet using the high tension electrostatic separation. Most of associated fine green silicate and quartz grains are removed in a tailing fraction. Most of the contaminated trace monazite grains, cassiterite and gold are included in the top strip tabled fraction in association with relatively finer rutile grains.

Individual minerals have been picked under the binocular microscope and the minerals identification was confirmed by X-ray diffraction (XRD). Scanning electron microscope (SEM) was used to study the picked mineral grains. A Philips SEM model XL30 equipped with an energy dispersive X-ray (EDX) unit was used. The dispersive electron probe microanalysis (EMPA) using a Cameca SX-100 microprobe at the Institute of Mineralogy and Crystal Chemistry, University of Stuttgart, Germany, was used for the analysis of the major oxides of some heavy minerals. The mean values of the probe microanalysis data of zircon, monazite, garnet, magnetite, ilmenite and rutile are given in Tables 1 and 2. Set of natural and synthetic reference materials were used for standardization and quantification. On the other hand, the analysis of the trace elements, including the rare earth elements (REE) in the separated heavy minerals was done by ICP-MS at ACME analytical labs, in Vancouver, Canada (Table 3).

**Table 1. Mean data of probe microanalysis of Mona-zite and zircon Concentrates from Rosetta.**

Oxides Wt. %	Monazite (n=219)	Zircon (n=200)	Oxides Wt. %	Monazite (n=219)	Zircon (n=200)
P2O5	29.84	<0.01	Sm <sub>2</sub> O <sub>3</sub>	2.15	<0.01
SiO <sub>2</sub>	0.79	31.83	Gd <sub>2</sub> O <sub>3</sub>	1.45	<0.01
ZrO <sub>2</sub>	0.01	66.40	Dy <sub>2</sub> O <sub>3</sub>	0.69	<0.01
HfO <sub>2</sub>	<0.01	1.44	Ho <sub>2</sub> O <sub>3</sub>	0.18	<0.01
ThO <sub>2</sub>	6.05	0.01	Er <sub>2</sub> O <sub>3</sub>	0.26	<0.01
UO <sub>2</sub>	0.06	0.03	Tm <sub>2</sub> O <sub>3</sub>	0.18	<0.01
Y <sub>2</sub> O <sub>3</sub>	1.99	0.03	Yb <sub>2</sub> O <sub>3</sub>	0.06	<0.01
La <sub>2</sub> O <sub>3</sub>	12.52	0.01	CaO	1.11	<0.01
Ce <sub>2</sub> O	27.32	0.01	Fe <sub>2</sub> O <sub>3</sub>	0.02	<0.01
Pr <sub>2</sub> O <sub>3</sub>	3.10	<0.01	PbO	0.21	<0.01
Nd <sub>2</sub> O <sub>3</sub>	11.10	<0.01			

**Table 2. Mean data of probe microanalysis of garnet, titanomagnetite, ilmenite and rutile concentrates from Rosetta.**

Oxides Wt. %	Garnet (n=38)	Ti-magnetite (n=180)	Ilmenite (n=300)	Rutile (n=160)
SiO <sub>2</sub>	53.21	0.22	0.39	0.25
Al <sub>2</sub> O <sub>3</sub>	29.98	1.51	0.15	0.09
FeO	42.23	74.62	46.53	1.04
MnO	7.88	0.54	1.19	<0.01
TiO <sub>2</sub>	0.06	19.94	49.19	98.44
CaO	5.11	0.03	0.04	0.04
MgO	3.75	1.53	1.82	0.01
ZnO	0.01	0.12	0.05	<0.01
V <sub>2</sub> O <sub>5</sub>	<0.01	0.82	0.50	<0.01
Cr <sub>2</sub> O <sub>3</sub>	<0.01	0.67	0.14	0.13

## Results and Discussions

### **Heavy Minerals; Source Versus Influx**

The fate of the heavy minerals and their changes in morphology and composition during the long transportation are discussed based on SEM and EMPA investigations on samples from Rosetta as an influx area and Blue Nile, Atbara, Sobat, Bahr El-Ghazal and White Nile as sources. The samples from the source areas have been selected from the known Shokri's collection. This collection was the main issue of detailed pioneer studies such as Shukri (1949 and 1951).

The comparison between heavy minerals in the influx and the sources reveals the following important assumptions:

1. Some minerals have entirely been lost during the long transportation. Barite is a good example, where it dominates in the heavy minerals composition of the Sobat system and other tributaries of Central Africa but it has not been encountered in the beach sediments of Rosetta (Plate 1, A & B). Barite in the source sediments is  $>200 \mu\text{m}$  in diameter and appears to be highly dissected and contains abundant inclusions of silicates. The barite fragile nature and its high specific gravity are the main reasons of its extinction in Rosetta beach sediments.
2. Minerals of low stability against chemical weathering such as pyrite and apatite come across the sediments of the Nile sources in Bahr El-Ghazal but never reach the influx (Plate 1, C & D).
3. Grains consisting of polycrystalline mineral clusters such as zircon from the White Nile and titano-magnetite from Atbara usually disintegrate into individual crystal up on the long transportation (Plate 1, E & F).
4. Abrasion polishes the surfaces of the heavy minerals and removes impurities. The mineral grains in the source areas are commonly contaminated by minerals at contact in their proximity (Plate 1, G & H).
5. The long exposure to the Nile water leads to dissolution along cleavage plane of minerals. This is best illustrated by the octahedral crystals of magnetite, which appear discrete in the sediments of the Blue Nile but corroded along the octahedral cleavage in beach sediments of Rosetta (Plate 2, A-E). The same phenomenon is valid for may other minerals especially the Fe-Ti minerals such as rutile, ilmenite (Plate 2, F-G), leucoxene, titano-magnetite and titanite.
6. The analysis by microprobe of many zircon grains from sources and influx (Table 4), suggests that the Zr/Hf ratio remains unaffected at almost chondritic level ( $\sim 30$ ). The composition of zircon from Rosetta seems to be an average of the source areas. The zircon-outsiders such as Fe, Ti, Al and Mg along with their empirical Si have been subtracted from the probe analysis data.

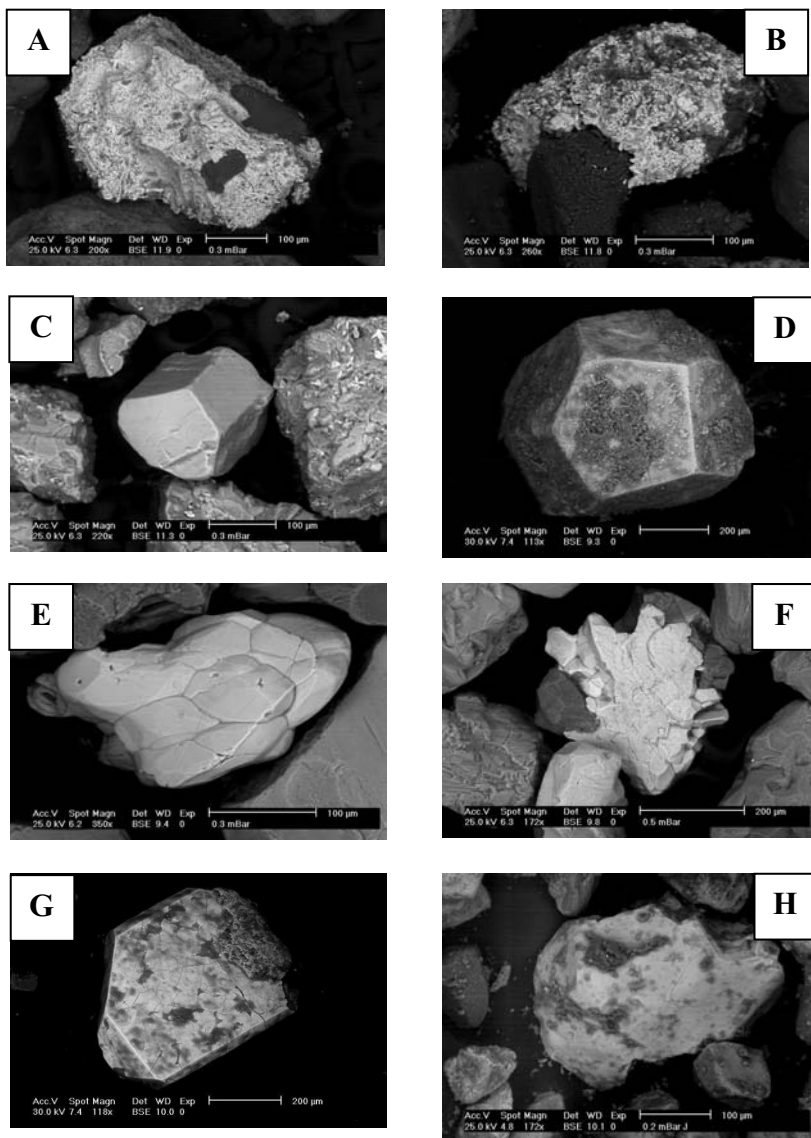


**Plate 1.** A and B: BSE images of microcrystalline barite from the Sobat system containing abundant silicate inclusions. C: BSE image of pseudohexagonal prismatic crystal of apatite displaying perfect crystal faces and edges from Atbara. D: BSE image of cubic crystal of pyrite (?) with almost fresh surfaces from Bahr El-Ghazal, suggesting very short proximity. E: BSE image of polycrystalline zircon from the White Nile. F: BSE image of polycrystalline titanomagnetite from Atbara. G and H: Zircon grains from Sobat tributaries before abrasion, where surfaces are highly tainted by silicate minerals.

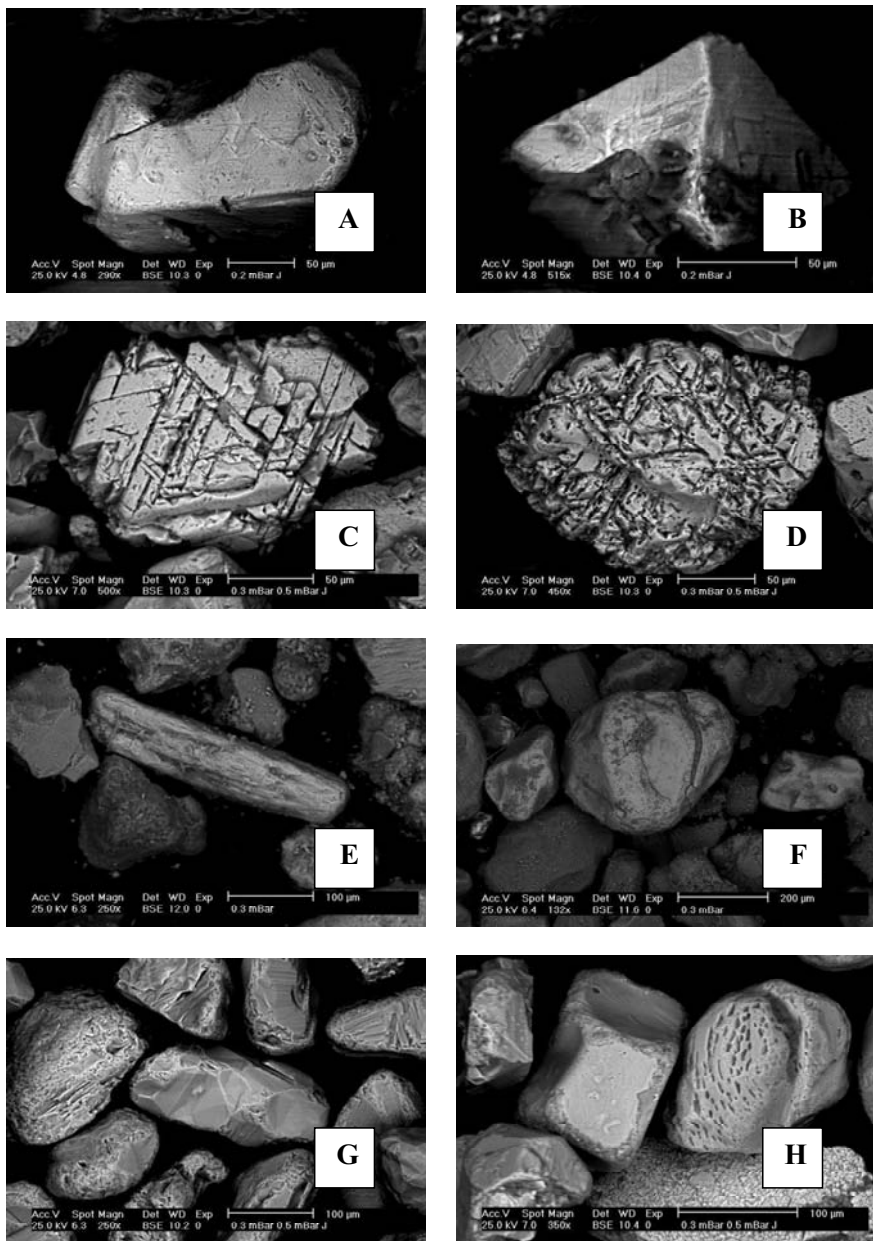


**Plate 2. A & B:** BSE images of solid octahedral grains of magnetite from the Blue Nile. **C & D:** BSE images of magnetite corroded along the octahedral cleavage from Rosetta. **E & F:** Ilmenite with contaminated surfaces from the Blue Nile. **H & G:** Polished ilmenite grains with abundant dissolution effect from Rosetta.

**Table 3. ICP-MS data of heavy minerals concentrate from Rosetta.**

Elements	Zircon	Monazite	Magnetite	Ilmenite	Rutile	Rutile*
Rb	0.35	0.9	2.2	0.85	0.5	0.4
Sr	12.15	86.1	26.3	15.17	23.5	20.6
Ba	46.5	7	41	38.17	32	24
Ga	1.1	<0.5	37.3	5.92	2.6	1.9
V	12	13	1841	629	616	1721
Co	0.5	0.4	34.5	19	1.2	3.4
Ni	0.5	0.5	111.5	3.13	0.9	1.4
Cu	1	0.6	62.4	2	7.1	2.7
Zn	3.5	5	341	11	8	20
Pb	1	83.3	11.1	5	1.8	8.5
As	<0.5	6.7	0.6	<0.5	<0.5	<0.5
Sn	13	3	5	6	258	3417
Se	0.5	6.9	0.6	<0.5	<0.5	<0.5
Au	1.4	<0.5	3.9	2.67	<0.5	7780
Hg	<.01	<0.01	<0.01	<0.01	0.01	2.16
W	1.6	1.8	<0.5	1	15.2	93.7
Zr	490000	794	1037	949	1126	4414
Hf	7773	<0.1	26	23.93	38.5	120
Nb	6.85	2.3	48.1	150	324	765
Ta	1.3	<0.1	2.7	6.43	4.3	41
Sc	104.5	54	13	33	39	51
Y	1119	14254	15	25	42.2	107
La	218	103426	19.7	35	40	571
Ce	441	226366	42	68	82.4	1096
Pr	51	25761	5.07	8.37	10	125
Nd	198.4	92500	21	32	38.2	456
Sm	41	18014	3.67	5.59	7	62
Eu	6	538	0.75	0.76	1.5	5
Gd	64	12211	4	5	6	44
Tb	14.1	1070	0.57	0.79	1.19	4.93
Dy	126	4033	3.03	4.58	7.39	23.14
Ho	38.68	475	0.6	0.94	1.47	3.87
Er	161.3	789	1.72	2.97	4.47	10.21
Tm	32.6	82.81	0.26	0.5	0.73	1.63
Yb	274	430	1.89	3.55	4.82	11.28
Lu	55.6	46.98	0.31	0.59	0.75	1.81
Th	223	53100	5.2	8.8	18.8	245.7
U	288	4103	3.5	13.45	30.4	85.6

\* Low grade rutile

After correction, zircon of Rosetta appears stoichiometric but with remarkable decrease in Hf. The Zr/Hf ratio increases (46) above the chondritic value (35) possibly due to selective dissolution of the heavier isovalent in the alkaline sea water. In general, radioactivity decreases in the zircons of Rosetta relative to those of the source areas. The SEM study suggests that the contaminating or inclusion materials are sometimes carriers of radioactivity.

**Table 4. Averages of microprobe analysis data of zircon from sources and influx.**

Oxides %	White Nile (n=10)	Sobat (n=9)	Blue Nile (n=8)	Rosetta (n=200)
ZrO <sub>2</sub>	64.74	64.84	64.45	66.40
HfO <sub>2</sub>	2.35	2.31	2.17	1.44
UO <sub>2</sub>	0.45	0.49	0.00	0.03
ThO <sub>2</sub>	0.48	0.00	0.00	0.01
SiO <sub>2</sub>	31.58	31.57	32.18	31.83

**Table 5. Mean data of probe microanalysis of monazite from White Nile and Rosetta, and calculated losses and gains.**

Oxides %	White Nile n=17	Rosetta n=219	Loss-Gain %
La <sub>2</sub> O <sub>3</sub>	15.35	13.28	-1.97
Ce <sub>2</sub> O <sub>3</sub>	29.20	28.97	0.00
Pr <sub>2</sub> O <sub>3</sub>	4.02	3.29	-0.70
Nd <sub>2</sub> O <sub>3</sub>	13.22	11.77	-1.35
Sm <sub>2</sub> O <sub>3</sub>	2.76	2.28	-0.46
Eu <sub>2</sub> O <sub>3</sub>	0.55	0.42	-0.13
Gd <sub>2</sub> O <sub>3</sub>	1.48	1.54	0.07
Y <sub>2</sub> O <sub>3</sub>	0.55	2.11	1.57
ThO <sub>2</sub>	6.14	6.10	0.00
UO <sub>2</sub>	0.68	0.06	-0.62
P <sub>2</sub> O <sub>5</sub>	26.04	30.20	4.40
Total			0.81

However, monazite grains have experienced more changes in composition, both in cationic and anionic positions. The monazites of the White Nile have been compared with those of Rosetta (Table 5). The monazite-outsiders count for about 47% of the average composition of the White Nile monazites but decreases to 1.34% for those of Rosetta. The average chondrite-normalized REE patterns show clear depletion in

the content of the analyzed REE, except Ce which seems to be immobile under the given weathering conditions (Fig. 2). The losses and gains of the monazite lattice are calculated assuming that Ce is immobile (Table 5). The obtained data suggest that Th is also immobile and most losses occur in the LREE (4.54%), except Ce. An important observation is the marked gain in Y and P<sub>2</sub>O<sub>5</sub> in the monazite of Rosetta which can be interpreted to development of xenotime solid solution during transportation or reaction with sea water. According to Ni *et al.* (1995) both monazite and xenotime structures have equal number of PO<sub>4</sub> tetrahedra and REO<sub>9</sub> polyhedra. Xenotime structure, however, possesses more regular polyhedron that accommodates the smaller HREE. Transformation on one structure into the other is possible, in spite of the voids in the xenotime structure. The solid solution between xenotime and

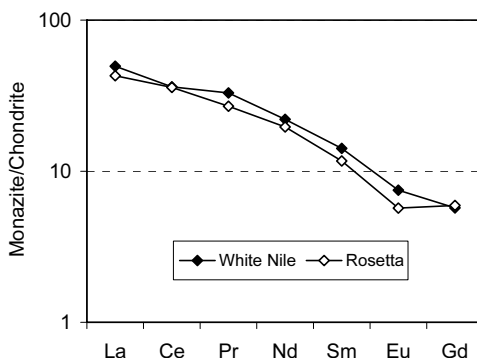


**Fig. 2. Average chondrite-normalized REE patterns of monazites from the White Nile and Rosetta.**

monazite has comprehensively been studied recently by Ondrejka, *et al.* (2007) and Moustafa (2009) along the Mediterranean beach of Egypt.

### ***Geochemistry of Heavy Minerals***

The following is brief discussion on the obtained data on the analyzed concentrates of minerals separated from the black sand of Rosetta. These minerals are of economic importance, such as; zircon, monazite, garnet, magnetite, ilmenite and rutile.

#### ***1. Zircon***

Zircon is a physically and chemically stable accessory mineral widely used for petrogenetic investigation in a variety of magmatic,

metamorphic, clastic sedimentary and hydrothermally altered rocks (Tomaschek, *et al.*, 2003; Hoskin, 2005). Zircon tends to incorporate trace elements useful as geochemical tracers (*e.g.*, REE, U, Th and Hf). Its alteration during alkali metasomatism of granites induces serious redistribution of these rare metals (El-Kammar and Mahdi, 2001). In the present study, zircon shows a distinct heterogeneity with respect to size, color, habit and composition (Plate 4). Such heterogeneity is possibly related to the provenance from which zircon was derived (Phllander, *et al.*, 1999). Zircon shape is controlled mainly by the chemistry, temperature and water content of the magma from which they crystallize (Pupin, 1980). The fine-grained zircon (259 $\mu\text{m}$ -108 $\mu\text{m}$ ) is euhedral where the (100) prism development is controlled by high temperature while the (110) by low temperature. Also bi-pyramidal (211) development is controlled by the chemistry of the alumina-rich magma (Plate 4, A-B). These crystal habits of the fine-grained zircon that vary from prismatic tetragonal, bi-pyramidal crystal to euhedral prismatic crystal reflect a magmatic origin.

Some angular to subangular fine grains of zircon are broken fragments of coarser size (Plate 4F). Few zircon grains are rounded to subrounded, elongated or spherical especially in the coarser size. The majority of such grains are colorless with high transparency. They attain brown and reddish brown colors. The metamict zircon, *i.e.*, is highly radioactive variety, has resinous luster (Plate 4D-E)) and some contain evacuated voids of inclusion precursors (Plate 4B-D).

The study of zircon in source areas documents the dominance of different inclusions of ilmenite, rutile and monazite. The probe microanalysis data (Table 1) suggest that the radioactivity of zircon is mainly related to uranium (0.03%) and it is generally depleted in Hf relative to Zr. The ICP-MS data (Table 3) confirm these observations and document even higher Zr/Hf ratio (63) and additional contribution of Th to the zircon radioactivity. The stability of Zr under the alkaline medium of the sea water is attributed by Magloughlin, *et al.* (2005) to complexing of hydroxide with Zr. However, Zr and Hf are not the only fractionated isovalues where Nb/Ta shows enrichment of the lighter isovalues while Y/Ho remains chondritic (29).

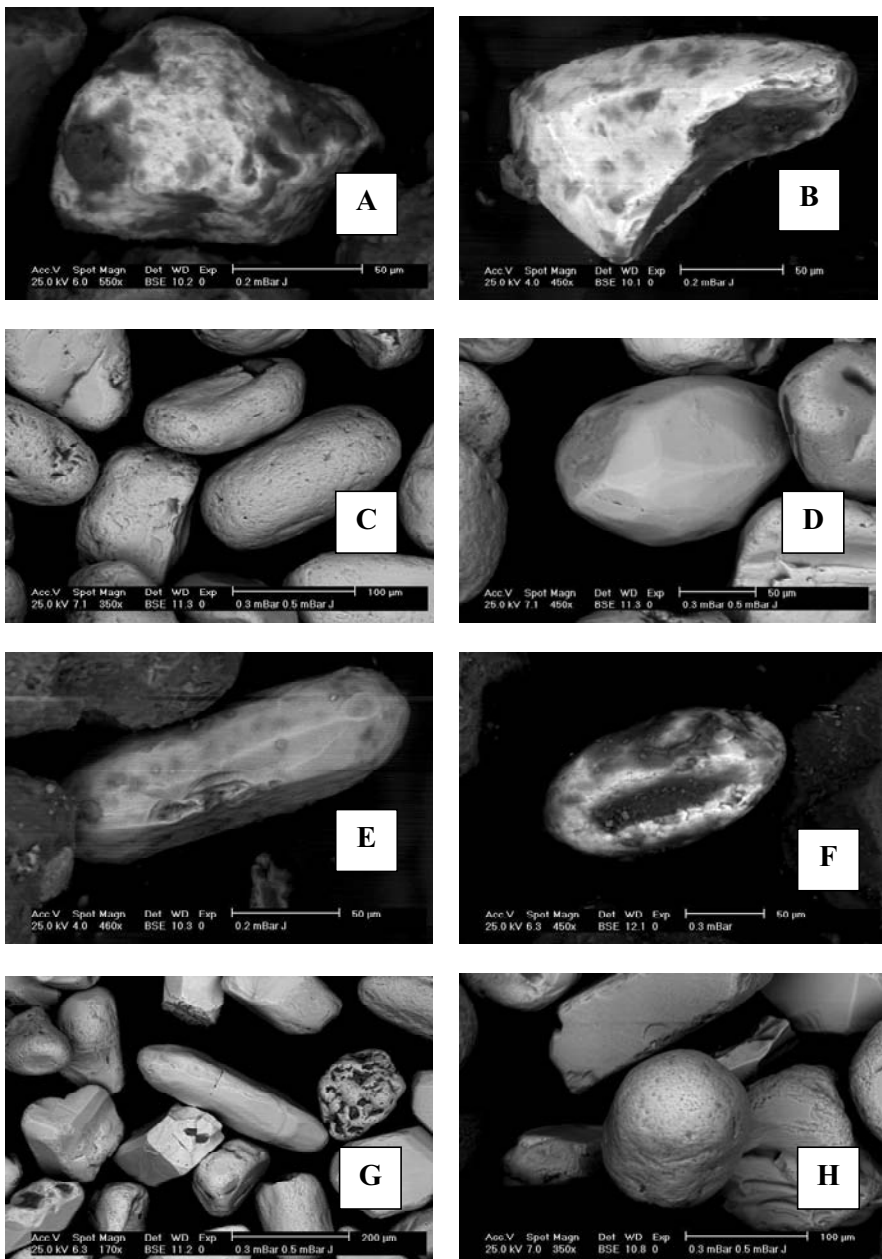
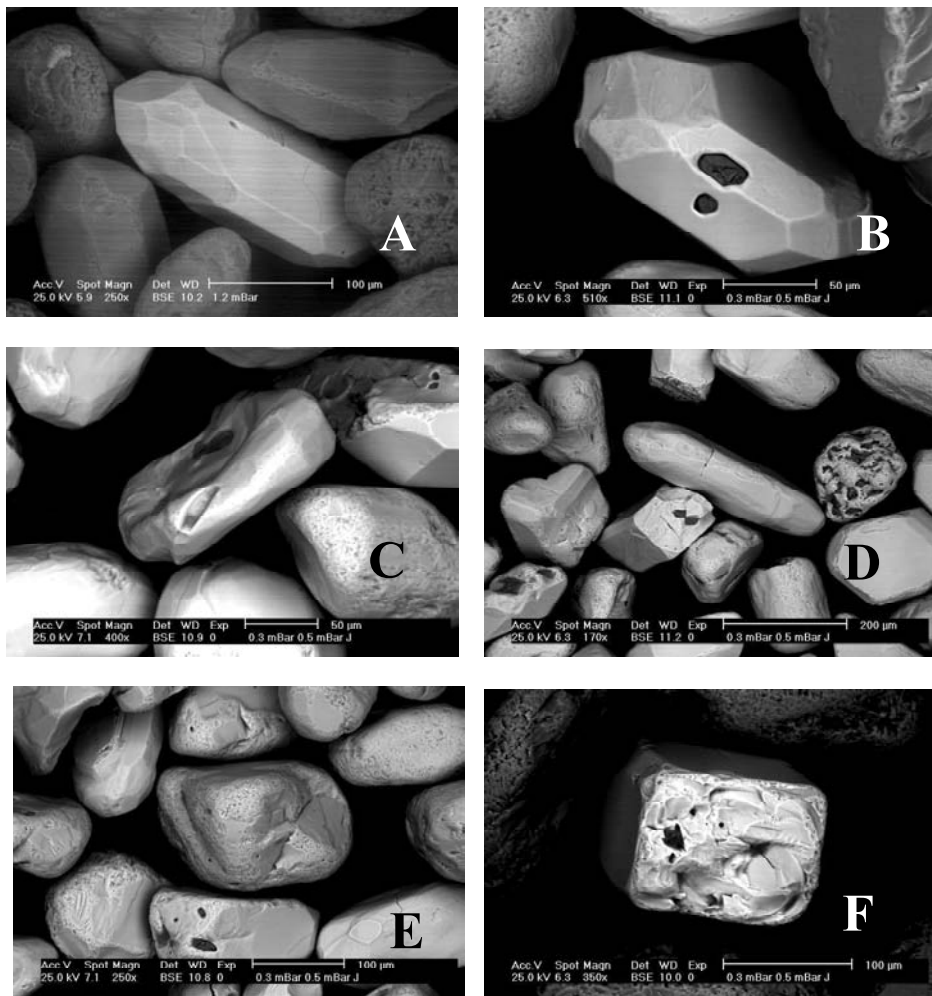


Plate 3. A & B: BSE images of subrounded monazite grains with contaminated surfaces picked from the White Nile sediments. C & D: BSE images of well rounded clean monazite grains from Rosetta. E & F: BSE images of markedly contaminated zircon grains from White Nile and Atbara, respectively. H & G: images of highly polished zircon grains from Rosetta.



**Plate 4. BSE images of different zircon habits encountered in the beach sediments of Rosetta. A. Prismatic and bipyramidal zircon of high elongation index (>3). B: Prismatic bipyramidal zircon with void spaces resulting from dissolution of less stable mineral inclusions. C and D: Well rounded zircon grains containing voids related to inclusion precursor. E: Well rounded grain of zircon displaying highly pitted and cracked surface. F: Coarse grain metamictic zircon broken along the basal pinacoid.**

Duddy and Kelly (1999) suggested discrimination between zircon derived from mantle and crust according to U content, where the latter is more U-rich. Based on EDX data on hundreds of zircon grains, high radioactivity (0.1-0.4%) characterizes the rounded coarse sized

( $>200\mu\text{m}$ ) variety of White Nile provenance. The fine-grained prismatic, bi-pyramidal zircon is diagnostically non-radioactive probably derived from the Ethiopian provenance.

The zircon concentrate contains 2800 ppm REE+Y (Table 3), with chondrite normalized pattern showing remarkable enrichment of the LREE which exceeds 950 ppm (Fig. 3). The unconventional aspect of the zircon pattern is further confirmed by a strong Eu deficiency ( $\Delta\text{Eu}=0.36$ ). This peculiar pattern of the zircon concentrate can be attributed to genetic controls, since no evidences of inclusions or replacement as deduced from the trace elements composition (Table 3). The unconventional REE pattern, the high radioactivity (233 ppm, U and 288 ppm, Th) and morphology suggest derivation of most zircon from highly fractionated felsic rocks. The fractionated Zr/Hf ratio (63) of zircon concentrate is rather related to long exposure with the alkaline sea water as witnessed by chondritic ratio ( $\sim 30$ ) in zircon from source areas (Table 5).

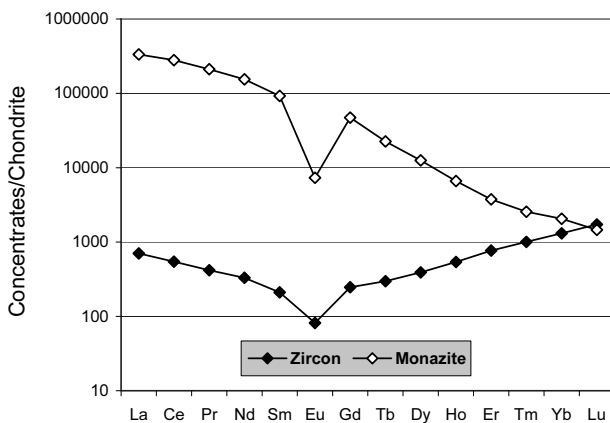


**Fig. 3. REE Chondrite-normalized patterns of zircon and monazite concentrates separated from the black sands of Rosetta.**

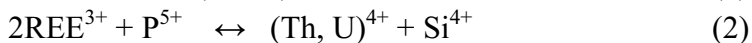
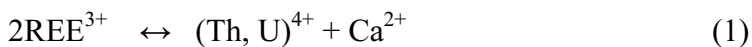
## 2. Monazite

Morphologically, the monazite grains display different levels of roundness but occasionally preserve the prismatic and bipyramidal habit. Some grains are broken into irregular shaped fragments while others are excessively dissolved under the control of the alkaline sea water (Plate 5A-D). The grains are mainly concentrated in the fine sand sizes. Some

large monazite grains are highly fractured. Moustafa, (2009) reported that the Egyptian beach monazite is colorless to pinkish in color and mostly derived from highly differentiated granite. He added that the prevailing monazite variety can be considered as a mixture of brabantite, xenotime and buttonite.

In the present study, the common variety of monazite appears to be resinous and commonly brown in color. The obtained data (Tables 1 and 3) suggest that they contain about 50% of REE+Y with marked predominance of the lightest four elements (La, Ce, Pr and Nd) which comprise more than 90% of the total REE budget. The abundance of the LREE is as follows; Ce > La > Nd > Pr > Sm > Eu. The chondrite-normalized REE pattern of the monazite concentrate reflects no positive anomaly of Ce, but the negative Eu anomaly is strongly imparting the whole pattern. The content of Th as a REE partner in monazite lattice is relatively low (5.31%). According to Mohanty, *et al.*, (2003), Th content is liable to decrease to very small values in the hydrothermal systems. Differentiation of alkali also produces Th-poor monazite from metaluminous to peraluminous granitic rocks.

The SEM examination suggests that subordinate variety of highly radioactive monazite containing more than 6% Th and possibly more than 006% U exhibits reddish colors. Moustafa, (2009) believes that this variety is product of hydrothermal alteration of preexisting minerals consortium that include monazite as well as HREE, Zr and U minerals. The compositional variations can also be explained in terms of ionic substitution, where the effective ionic size and charge are the governing factors. These compositional variations are controlled by the possible substitution of the REE by Th and U as proposed by Van Emden, *et al.* (1997):



The absence of curvilinear zonation in the studied monazite grains may support, according to Harlov, *et al.*, (2007), derivation from granitic and pegmatitic province and not metamorphic ones. Further, in agreement with Seydoux-Guillaume, *et al.* (2007) and Dawood and Abd El Naby (2007), the presence of thorite inclusions favors derivation from granite and pegmatite. Moreover, El-Kammar, *et al.* (1992) stated that the monazite is almost exclusively supplied by the White Nile.

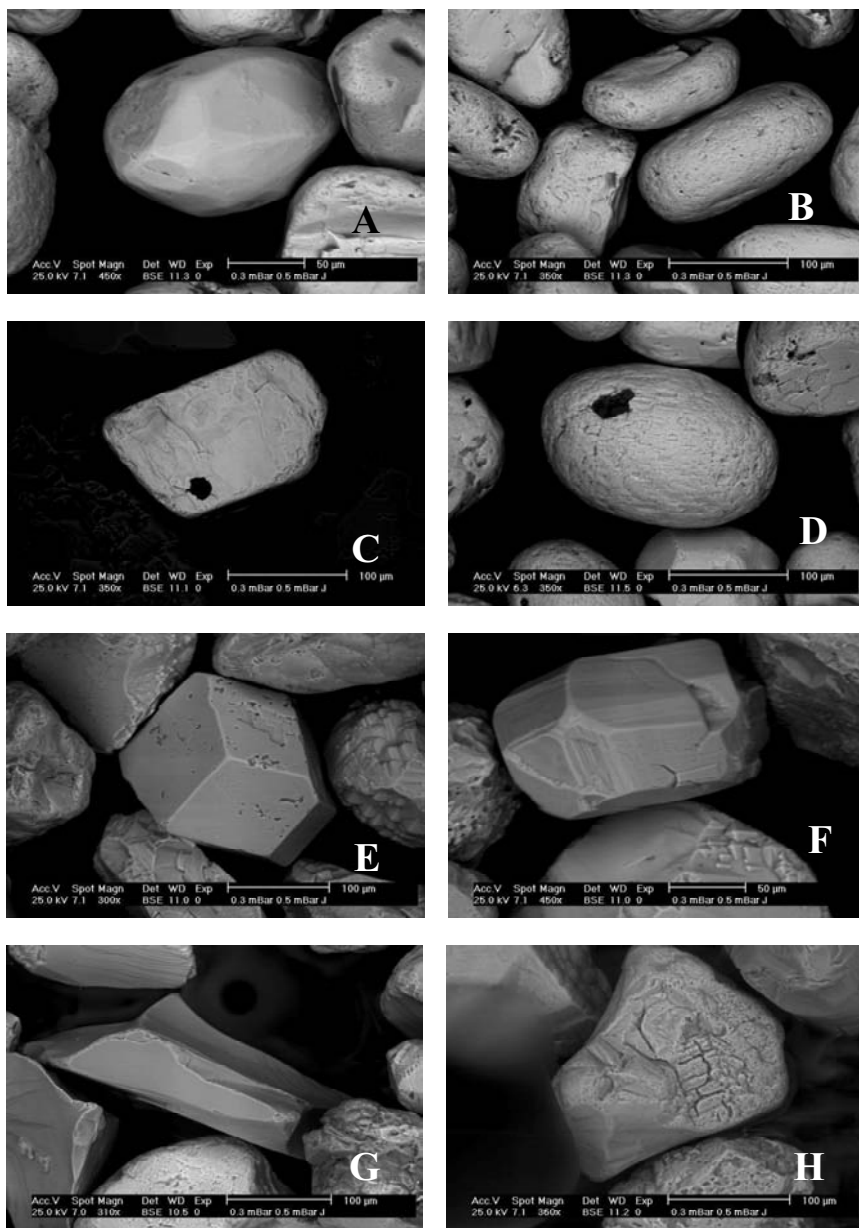


**Plate 5. BSE images of monazite (A-D) and garnet (E-H) from the beach sediments of Rosetta. A: Prismatic-bipyramidal monazite with clear surfaces. B: Well rounded and pitted surface monazite. E and F: Excessive dissolution of subangular and well rounded monazite. E and F: Euhedral rhombohedral garnet. G: Angular almandine garnet lacking crystal faces. H: Dehydration cracks of the gelatinized surface of spessartine garnet.**

### 3. Garnet

Garnet is a common mineral of metamorphic rocks such as gneiss and schist of all composition from basic to acid, crystalline limestone and pegmatites. The studied garnet occurs in the fine sand size followed by the medium sand size. Based on composition, garnet follows the order of abundance; almandine > spessartine > pyrope > grossularite but solid solution phases are occasionally encountered (Table 2). Garnet grains are angular to subangular, irregular to rounded, and rhombic-dodecahedron to octahedron (Plate 4, E-H). The encountered garnets are commonly reddish-brown to almost black in color.

Using the average EMPA analysis data of 38 garnet grains given in Table 2, the chemical formula is calculated to be;  $(\text{Fe}^{2+})_{2.031}, \text{Mg}_{0.323}, \text{Mn}_{0.386}, \text{Ca}_{0.131}) (\text{Al}_{2.041}, \text{Ti}_{0.003}) (\text{SiO}_4)_{3.075}$ . This composition corresponds to the following end members; 70.9% almandine, 13.4% spessartite, 11.2% pyrope and 4.51% grossularite. The predominance of almandine garnet suggests main supply from pelitic schist. However, the high spessartine content is probably related to garnet from pegmatite as described by Thoni and Miller (2000) and Zhang, *et al.* (2001).

The EDX data, although of low precision, suggest that the studied garnet is occasionally radioactive due to Th which may reach about 1%. Salah, *et al.* (2005) found that garnet of Rosetta is characterized by relative enrichment of the HREE over the LREE with prominent negative Eu anomaly. El-Kammar, *et al.* (1992), Garzanti, *et al.* (2006) and others agree that garnet is mostly derived from metamorphic basement passing through the White Nile.

### 4. Opaque Minerals

The opaque minerals are mainly represented by spinel and ilmenite, mostly concentrated in the very fine sand and silt size fractions. The magnetic opaques are represented by chromopicotite, magnetite and ilmenite. The opaque minerals range in color from brownish to black, and generally rounded to subangular. Magnetite displays an octahedral form while ilmenite, leucoxene and rutile lack clear crystal forming display subangular to subrounded habit (Plate 6).

The qualitative EDX analysis data of the opaque minerals indicate that chromopicotite contains 45%  $\text{Cr}_2\text{O}_3$ , 32%  $\text{FeO}$ , 8%  $\text{Al}_2\text{O}_3$  and 6%  $\text{MgO}$ , in average of 20 grains. In all cases  $\text{TiO}_2$  is about 1% and  $\text{CaO}$  is minor constituent.

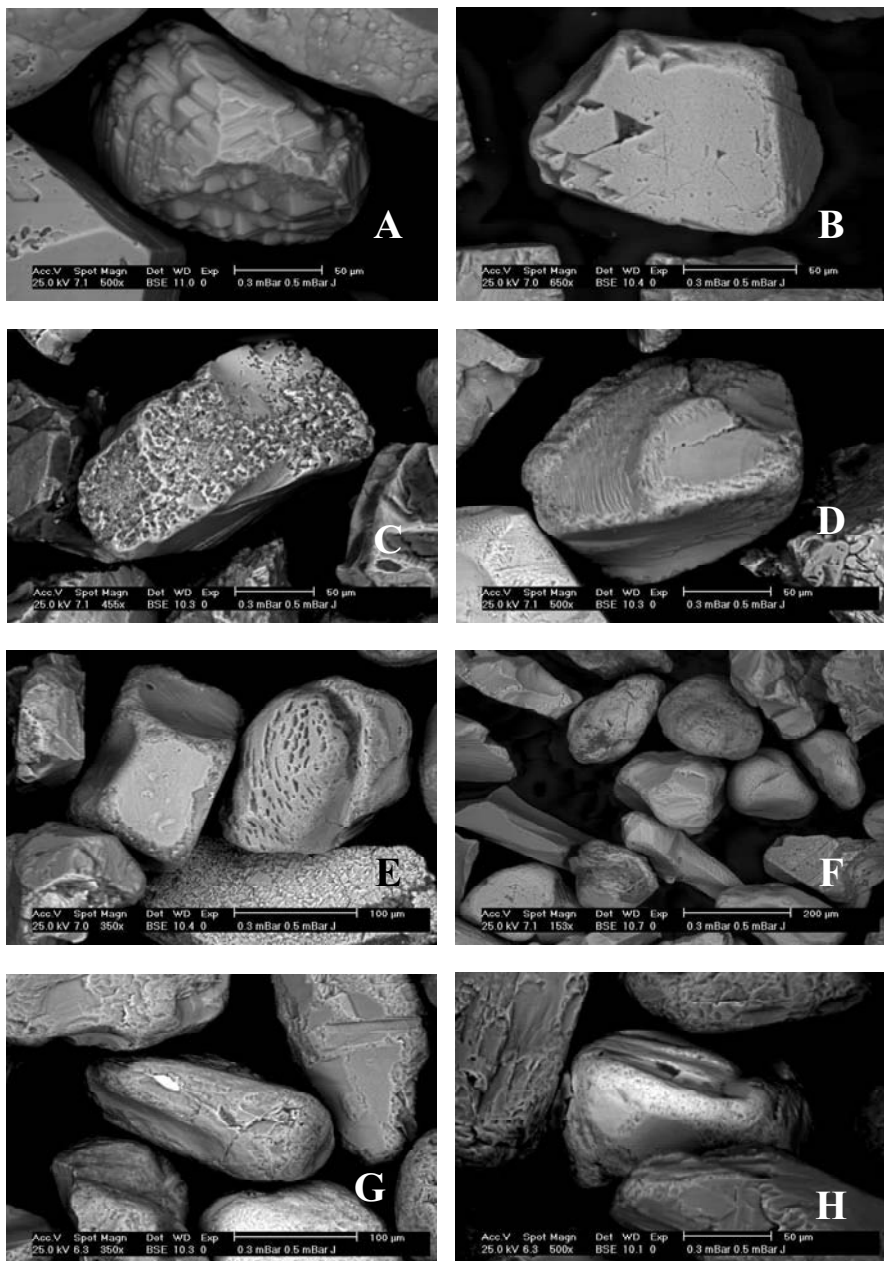


**Plate 6. BSE images of various opaque minerals separated from the heavy minerals of Rosetta beach sediments. A and B magnetite grains displaying an octahedral pattern and strongly affected by dissolution. C and D: subrounded ilmenite grains. E and F: subrounded leucoxene grains. G and H: Well-rounded rutile grains containing inclusions (bright colored) of monazite.**

### Magnetite-Titanomagnetite

The non-discrete varieties of magnetite are the most dominant. The EMPA data show that the content of  $\text{TiO}_2$  in the magnetite ranges from 0.22 to 56% averaging 19.94% and the total iron content as  $\text{FeO}$  content ranges from 42% to 92.68% averaging 74.62% (Table 2). This represents complete solid solution between magnetite and ilmenite. The average contents of  $\text{MgO}$ ,  $\text{Al}_2\text{O}_3$ , and  $\text{MnO}$  are 1.53, 1.51 and 0.54%, respectively (Table 2). The ICP data indicate that magnetite concentrates are sizeable group of elements (Table 3). It contains 1841 ppm V, 112 ppm Ni, 341 ppm Zn, 62 ppm Cu, 3.9 ppm Au and 1037 ppm Zr (Table 3). According to Wolfenden, *et al.* (2005) and Garzanti, *et al.*, (2006), and in agreement with the pioneer conclusion of Shukry (1949 and 1951), these titanomagnetites are derived from the basic volcanic rocks of the Blue Nile provenance. Also, in agreement with El-Kammar, *et al.* (1992), the high heavy metals content (V, Zn, Ni, and Cu) is indicative of the basic volcanic source.

Magnetite has relatively high REE budget (104.5 ppm) with predominance of the LREE over the HREE ( $\text{LREE/HREE} = 2.8$ ). The chondrite normalized pattern of magnetite displays also clear negative anomaly of Eu (Fig. 4). The high REE budget, relative enrichment of the LREE, depletion in Eu and the very high content of Zr (1037 ppm) are strong evidence of potential contamination by fine inclusions of other minerals such as zircon and monazite. However, in all cases, the ratios of the isovalents, *e.g.*,  $\text{Zr/Hf}$  (40),  $\text{Nb/Ta}$  (18) and  $\text{Y/Ho}$  (25), are within the chondritic limits. The radioactivity which is related to both Th (5.2 ppm) and U (3.5 ppm) is also provoked by the same inclusions.

### Ilmenite

The Fe-Ti minerals such as ilmenite and leucoxene are rounded and their surfaces are strongly pitted due to dissolution during transportation (Plate 6, C-F). The average composition of 300 grains from the ilmenite concentrate as analyzed by the microprobe indicates that  $\text{TiO}_2$  and  $\text{FeO}$  constitute 49.19 and 46.53%, respectively while  $\text{MgO}$  and  $\text{MnO}$  represent 1.82 and 1.19%, respectively (Table 2). Similar to magnetite, ilmenite accumulates high concentrations of many trace elements such as 629 ppm V, 949 ppm Zr, 150 ppm Nb, 196 ppm REE and 13.5 ppm U (Table 3). This agrees with Dewedar, (1997) who recorded high values of Y, Nb, and Zr and low concentration levels of Sr,

Ba, Co, Zn Sc, Y and Th in the ilmenite of Rosetta. This is interpreted to fine inclusions of accessory minerals in ilmenite. However, Pearce (1990) explained the presence of Nb in ilmenite due to the Nb substitutes for Ti in the octahedral sites. In the present work, the chondritic Zr/Hf and Y/Ho ratios (40 and 27, respectively) suggest an orthomagmatic origin.

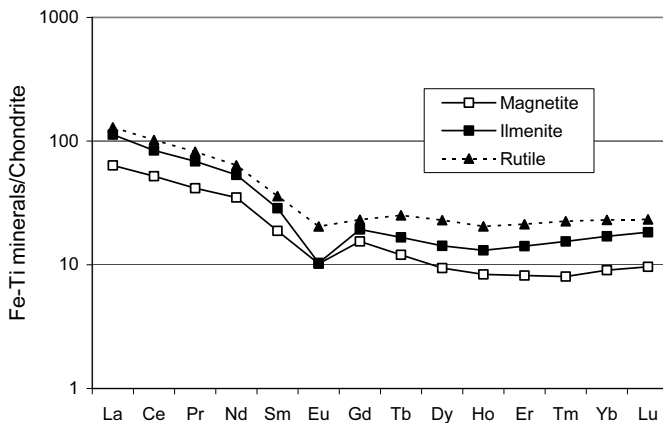


**Fig. 4.** REE Chondrite-normalized REE patterns of magnetite, ilmenite and rutile separated from the black sands of Rosetta.

The REE budget of the ilmenite concentrate is estimated to be 171 ppm, in addition to 25 ppm Y and 33 ppm Sc (Table 3). The chondrite-normalized REE pattern of ilmenite displays the relative enrichment in LREE due to the abundant inclusions of monazite (Fig. 4). This is confirmed by the relative enrichment in LREE while ilmenite is supposed to be relatively enriched HREE (Nakamura, *et al.* 1986).

#### Rutile

The majority of rutile particles behave as conductors (Moustafa, 1995). Two main rutile varieties have been recognized, namely; primary and secondary. The first variety displays different colors ranging from yellow to black, and exhibits different degrees of roundness ranging from angular to well-rounded. The secondary rutile variety represents about 6% of the bulk-high grade rutile concentrate, essentially composed of  $\text{TiO}_2$  with little iron. This variety of rutile has different colors ranging from yellowish to brown white and its grains have different degrees of roundness (Plate 6, G-H).

The average  $\text{TiO}_2$  content in rutile, based on 160 probe microanalysis on grains picked from the black sands of Rosetta, is 98.44% with 1.04%  $\text{FeO}$  and 0.13%  $\text{Cr}_2\text{O}_3$  (Table 2). Two rutile concentrates are analyzed by ICP-MS (Table 3). The low purity concentrate contains abnormally high contents of heavy metals (*e.g.*, 1721 ppm V and 3412 ppm Sn), high field strength elements (*e.g.*, 1126 ppm Zr and 765 ppm Nb), rare earth elements (2528 ppm) and gold (7780 ppb). This means that the low grade rutile contains potential concentrations of rare metals due to impurities of key minerals such as cassiterite, zircon, monazite, columbite and gold.

The low grade rutile is highly radioactive where Th measures 246 ppm while U is 86 ppm. The high Th content and the marked enrichment of the LREE over the HREE, where lightest four REE (*i.e.*, La, Ce, Pr and Nd) constitute about 90% of the total REE budget suggest abundant monazite impurities (Plate 6G). The chondrite-normalized REE pattern confirms this statement. The comparison between the chondrite normalized patterns of the low and high grade rutile, suggests that the former displays clear monazite signature (Fig. 5). Both low and high grades of rutile concentrates exhibit marked Eu deficiency, although stronger for the low grade ( $\Delta\text{Eu} = 0.3$ ) possibly due to formation from highly fractionated magma.

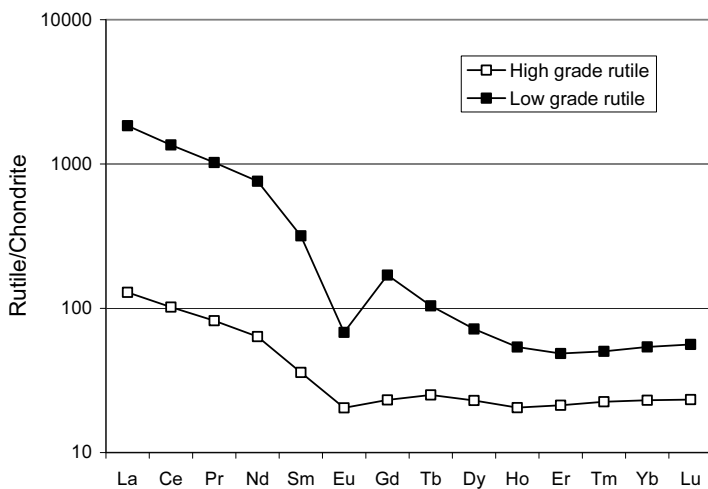


Fig. 5. REE Chondrite-normalized REE patterns of low grade and high grade rutile separated from the black sands of Rosetta.

## Conclusion

The River Nile drains its heavy minerals content from different sources along its course from the central and eastern parts of Africa in the south to the Mediterranean Sea in the North. The huge black sand reserves involve economic metals-rich heavy minerals such as zircon, monazite, garnet, magnetite, ilmenite and rutile (more than 3% by weight). The content varies from place to place but the highest potential is located close to the outlets of the River Nile in Rosetta.

In this study, seven samples were collected from the highly concentrated black sand on a grid pattern of 200m - 100m and the drilling to 5 meters depth in a total area of about 2km<sup>2</sup>. The separation of individual heavy minerals concentrate was done by the Wilfley shaking tables for wet-gravity concentration using electrostatic and magnetic separators. Concentrates of zircon, monazite, garnet, magnetite, ilmenite and rutile were exclusively analyzed by SEM, EMPA and ICP-MS.

The comparison between heavy minerals in source areas and influx highlights the destiny of these minerals and their changes in morphology and composition during the long transportation. Brittle and metastable minerals (*e.g.*, barite and pyrite) are entirely lost and never reached the influx while polycrystalline grains are disintegrated. Abrasion polishes the surface of the heavy minerals and dissolution takes place along cleavage planes. The ultrastable minerals as zircon and monazite experienced changes in their composition.

Heterogeneity in zircon covers all aspects including; color, morphology, size, elongation index, radioactivity and composition. However, radioactivity discriminates the uraniferous zircon of the White Nile from the non-radioactive variety of the Ethiopian province. The separated zircon concentrate is strongly imparted by the White Nile variety. This is further confirmed by the chondrite-normalized REE pattern that displays marked enrichment in REE with strong Eu deficiency. Monazite is commonly brown in color, resinous and rounded in shape mostly derived from granitic province. REE+Y constitute half of its weight with marked predominance of the lightest four elements (La, Ce, Pr and Nd) which comprise more than 90% of the total REE budget. Garnet dominates in the fine and medium sand sizes with angular to subrounded aspect, sometime displaying rhombic-dodecahedron to octahedron crystal form. It has composition corresponds to the following

end members; 70.9% almandine, 13.4% spessartite, 11.2% pyrope and 4.51% grossularite. The predominance of almandine garnet suggests main supply from pelitic schist.

The titano-magnetite minerals such as magnetite, ilmenite and leucoxene are mainly derived from the mafic volcanic rocks of the Blue Nile provenance. Magnetite concentrate contains high concentrations of heavy metals such as V (1841 ppm), Ni (112) ppm, Zn (341 ppm) and Cu (62 ppm), but also contains 3.9 ppm Au and 1037 ppm Zr. Similar observations are also recorded for ilmenite and rutile. The low grade variety of the latter is even richer in Zr, Nb, REE and Au. The chondrite-normalized REE patterns of the opaque heavy minerals (magnetite, ilmenite and rutile) indicate impurities of rare metals bearing minerals such as cassiterite, zircon, monazite, columbite and gold.

### References

- Anwar, Y.M. and El Bousiely, A.M.** (1970) Subsurface studies of the black sand deposits at Rosetta Nile mouth, Egypt. *Bull. Fac. Sci. Alexandria Univ., Egypt*, **10**: 141-150.
- Basu, A. and Molinaroli, E.** (1989) Provenance characteristics of detrital opaque Fe-Ti oxide minerals. *J. Sed. Petrol.*, **59** (6): 922-934.
- Dabbour, G.A.** (1995) Estimation of the economic minerals reserves in Rosetta beach sands. *Egypt. Min.*, **7**: 153-166.
- Dabbour, G.A.** (1997) Mineralogical study on the opaque minerals and secondary rutile from the Egyptian black sands. *Proceed. Egypt Acad. Sci.*, **47**: 105-121.
- Dawood, Y.H. and Abd El-Naby, H.H.** (2007) Mineral chemistry of monazite from the black sand deposits, northern Sinai, Egypt: a provenance perspective. *Mineralogical Magazine*, **71** (4): 441-458.
- Duddy, I. R. and Kelly P. R.** (1999) Uranium in mineral sands. *Austral. Instit. Geosci. Bul.*, **26**.
- El Hadry, A.F.** (1988) Geologic and radiometric investigations on Abu Khashaba deposits, east Rosetta, Egypt. *M.Sc. Thesis*, Fac. Sci., Cairo Univ., Egypt.
- El Hadry, A.F.** (1998) Geological, sedimentological and radiometric studies on the black sand deposits, west Rosetta beach with emphasis on the heavy economic minerals. *Ph.D. Thesis*. Fac. Sci., Cairo Univ., Egypt.
- El Shazly, E.M.** (1965) *Thorium resources in the United Arab Republic and their possible utilization*. Panel on utilization of Th in power reactors, IAEA, Vienna, pp: 186-198.
- El Shazly, E.M., El Sokkary, A.A. and Dabbour, G.A.** (1981) Distribution of beach zircon along the Mediterranean Coast, Egypt. *Egypt. J. Geol.*, **25**, 1-2.
- El-Kammar, A.A. and Mahdi, I.A.** (2001) Changes occurring in accessory minerals during alkali-metasomatism of granites from Egypt: An environmental scanning electron microscope study. *Egypt. J. Geol.*, **46** (1): 167-182.
- El-Kammar, A.A., Philip, G. and Arafa I.** (1992) Geochemistry of Recent Nile sediment from the main Nile course in Egypt and the principle tributaries in Ethiopia and Sudan. *Proceeding of the 1<sup>st</sup> International conference on the Geology of the Arab Word, Cairo Univ.*, pp: 527-541.
- Garzanti, E., Ando, S., Vezoli, G., Abdel Megid, A.A. and El-Kammar, A.** (2006) Petrology of Nile River sands (Ethiopia and Sudan): Sediment budgets and erosion patterns. *Earth and Planet. Sci. Let.*, **252**: 327-341.

- Harlov, D.E., Wirth, R. and Hetherington, C.J.** (2007) Replacement of monazite by a huttonite component: nature and experiment. *Am. Min.*, **92**: 1652-1664.
- Hoskin, P.W.O.** (2005) Trace-element composition of hydrothermal zircon and the alteration of Hadean zircon from the Jack Hills, Australia. *Geochim. Cosmochim. Acta*, **69**: 637-648.
- Jones, A.P., Wall, F. and Willianmas C.T.** (1996) *Rare earth minerals: Chemistry. Origin and ore deposits*. The Min. Soci. series 7, Chapman and Hall.
- Magloughlin, J.F., Merkel, I.S., and Koenig, A.** (2005) *Zircon aqueous solubility and partitioning systematic*. Goldschmidt Conference Abstracts, Accessory Mineral Geochemistry.
- Mohanty, A.K., Das, S.K., Vijayan, V., Sengupta, D. and Saha, S.K.** (2003) Geochemical studies of monazite sands of Chhatrapur beach placer deposit of Orissa, India by PIXE and EDXRF method. *Nuclear Instruments and Methods in Physics Research Section B: Beam Interaction with Materials and Atoms*, **211**: 145-154.
- Moustafa, M.I.** (1995) Investigations of some physical properties of zircon and rutile to prepare high purity mineral concentrates from black sand deposits, Rosetta, Egypt. *M.Sc. Thesis. Fac. Sci., Mansoura Univ., Egypt*, 158p.
- Moustafa, M.I.** (2007) *Geochemical studies of the Egyptian beach cassiterite concentrate and its importance as a source for Sn, Ta, Nb and others*. 1, III, 63-78, Assuit, Egypt.
- Moustafa, M.I.** (2009) Mineralogical and geochemical studies on monazite - REE silicate series in the Egyptian beach monazite concentrate. *Egypt. Sed.*, **17**: 63-88.
- Nakamura, Y., Fujimaki, H. and Nakamura, N.** (1986) Hf, Zr, and REE partition coefficients between ilmenite and liquid: Implications for lunar petrogenesis. *J. Geophys. Res.*, **91**: 219.
- Ni, Y., Hughes, J.M. and Mariano, A.N.** (1995) Crystal chemistry of the monazite and xenotime structures. *Am. Min.*, **80**: 21-26.
- Ondrejka, M., Uher, P., Prek, J. and Ozdin, D.** (2007) Arsenian monazite-(Ce) and xenotime-(Y), REE arsenates and carbonates from the Tisovec-Rejkovo rhyolite, Western Carpathians, Slovakia: Composition and substitutions in the (REE, Y)  $XO_4$  system ( $X=P$ , As, Si, Nb, S). *Lithos*, **95**: 116-129.
- Pearce, N.J.** (1990) Zirconium and niobium-bearing ilmenites from the Igalko dyke swarm, South Greenland. *Min. Mag.*, **54**: 585-588.
- Phllander, C., Rozendaal A. and de Meller R.J.** (1999) Characteristics of zircon in Placer Deposits along the West Coast of South Africa. *S African J. Sci.*, **95**: 381-386.
- Pik, R., Deniel, C., Coulon, C., Yirgu, G., Hoffman, C. and Ayalew, D.** (1998) The northwestern Ethiopian Plateau flood basalts: classification and spatial distribution of magma types. *J. Volcan. Geoth. Res.*, **81**: 91-111.
- Pupin, J.P.** (1980) Zircon and granite petrology. *Contrib. Min. Petrol.*, **73**: 207-220.
- Salah, S.S.; Ammar, F.A.; Mira, H.I. and Abdou, N.A. 2005: Mineralogical and sedimentological characters of Garnets from west Rosetta, Egypt. *Sedimentology Egypt*, **13**: 133-150.
- Seydoux-Guillaume, A., Wirth, R. and Ingerin, J.** (2007) Contrasting response of ThSiO<sub>4</sub> and monazite to natural irradiation. *Europ. J. Min.*, **19**: 7-14.
- Shukri, N.M.** (1949) The mineralogy of some Nile sediments. *Quat. J. Geol. Soc., London*, **105**: 511-534.
- Shukri, N.M.** (1951) Mineral analysis tables of some Nile sediments. *Bull. Inst. Desert d' Egypt*, **1(1)**: 39-67
- Tadesse, S., Milesi, J.P. and Deschamps, Y.** (2003) Geology and potential of Ethiopia: a note on geology and mineral map of Ethiopia. *J. African Earth Sci.*, **36**: 273-313.
- Thoni, M. and Miller, Ch.** (2000) Permo-Triassic pegmatites in the Alpiae eclogite-facies koralpe complex. Austria age and magma source constraints from mineral chemicals Rb-Sr and Sm-Nd isotope data. *Schweiz. Min. Petrogr. Mitt.*, **80** (2): 169-186.

- Tomaschek, F., Kennedy, A.K., Villa, I.M., Lagos, M. and Ballhaus, C.** (2003) Zircons from Syros, Cyclades, Greece-recrystallization and mobilization of zircon during high-pressure metamorphism, *J. Petrol.* **44**: 1977-2002.
- Van Emden, B., Thornber, M.R., Graham, J. and Lincoln, F.J.** (1997) The incorporation of actinides in monazite and xenotime from placer deposits in Western Australia. *The Canad. Min.*, **35**: 95-104.
- Wolfenden, E., Ebinger, C., Yirgu, G., Renne, P. and Kelley, S.P.** (2005) Evolution of a volcanic rifted margin, Southern Red Sea, Ethiopia. *Bulletin of the Geological Society of America*, **117**: 846-864.
- Zhang, Ch., Giere, R., Srnitz, H., Brack, P. and Ulmer, P.** (2001) Garnet-quartz intergrowths in granitic prgmatites from Bergell and Adamello, Italy. *Schweiz. Min. Perogr. Mitt.* **81**: 89-113.

## جيوكيمياء المعادن الثقيلة الاقتصادية في الرمال السوداء

### برشيد، مصر

**أحمد الكمار، و عبلة رجب<sup>\*</sup>، و محمد إسماعيل مصطفى<sup>\*</sup>**

قسم الجيولوجيا، كلية العلوم، جامعة القاهرة

**\* هيئة المواد النووية المصرية، القطامية**

المستخلص. تمت دراسة مصادر المعادن الثقيلة الهامة باستخدام تقنيات بحثية متنوعة مثل الميكروскоп الضوئي، وأشعة الحيود السينية، والميكروскоп الماسح الإلكتروني والمسبار الإلكتروني وتحليل طيف الكتلة بالبلازما التأثيرية. تم ذلك على ركاز المعادن الثقيلة والتي تم فصلها بطرق الجاذبية الرطبة وفقاً للخصائص المغناطيسية والكهربائية للمعادن. كما تمت المقارنة بين بعض المعادن مثل الزيركون والمونازيت والجارنت والمجنيت والإلمنيت والروتيل في الركاز المفصول من رمال رشيد، ونفس المعادن عند منابع النيل، لتقدير تأثير النقل لمسافات طويلة. في هذا الخصوص تم توظيف عينات شكري المعروفة، والتي تم توصيفها بكل دقة في نصف القرن الماضي.

بصورة عامة تصبح أسطح المعادن أكثر صفاءً، وتحرر من الشوائب نتيجة للنقل الطويل، بينما تفقد بعض المعادن بصورة كاملة. بيد أن المعادن الثقيلة المعروفة ببنائها العالي للتجوية والنقل مثل الزيركون، فإنها ليست بعيدة عن التأثر. دلت جيوكيمياء العناصر الأرضية النادرة على أن الزيركون جاء من منابع النيل الأبيض من صخور جرانيتية متمايزه وبجمانيت متغير. كما أمكن تمييز نوعين

من المونازيت هما عالي ومنخفض التوريوم، وهما من نواتج الصخور الفلسية المتمايزة.

يتبع الجارنت، في أغلبه، نوع الألمندين وهو ذو أصل متحول لصخور الشيسست، ويأتي مع رواسب النيل الأبيض. ولكن المعادن المعتمة الثقيلة مثل الماجنيت والإلمنيت والروتنيل فهى من نواتج النيل الأزرق، حيث تأتى من صخور البازلت القاعدية في الهضبة الأثيوبية. وتحتوي ركاز هذه المعادن على نسب عالية من عناصر هامة مثل الذهب (تركيز يصل إلى ٧٧٨٠ جزء في البليون) كما تحتوي على تركيز عالى من عناصر الزيركونيوم والقصدير وإشعاع عالى نتيجة للشوائب.